Journal of the Serbian Chemical Society
JSCS-info@shd.org.rs • www.shd.org.rs/JSCS

J. Serb. Chem. Soc. *78* (11) 1703–1716 (2013)
JSCS–4528

UDC 547.261+66.094.3+546.92:
544.4+621.352
Original scientific paper

Electrochemical oxidation of methanol on Pt/$(Ru_xSn_{1-x})O_2$ nanocatalyst

MILA N. KRSTAJIĆ[1#], MAJA D. OBRADOVIĆ[2#], BILJANA M. BABIĆ[3], VELIMIR R. RADMILOVIĆ[1], UROŠ Č. LAČNJEVAC[4], NEDELJKO V. KRSTAJIĆ[1] and SNEŽANA Lj. GOJKOVIĆ[1*#]

[1]Faculty of Technology and Metallurgy, University of Belgrade, Karnegijeva 4, 11000 Belgrade, Serbia, [2]Institute of Chemistry, Technology and Metallurgy, University of Belgrade, Njegoševa 12, 11000 Belgrade, Serbia, [3]Vinča Institute of Nuclear Sciences, University of Belgrade, P. O. Box 522, 11001 Belgrade, Serbia and [4]Institute for Multidisciplinary Research, University of Belgrade, Kneza Višeslava 1, 11030 Belgrade, Serbia

(Received 18 July, revised 4 September 2013)

Abstract: Ru-doped SnO_2 powder, $(Ru_xSn_{1-x})O_2$, with a Sn:Ru atomic ratio of 9:1 was synthesized and used as a support for Pt nanoparticles (30 mass % loading). The $(Ru_xSn_{1-x})O_2$ support and the Pt/$(Ru_xSn_{1-x})O_2$ catalyst were characterized by X-ray diffraction measurements, energy dispersive X-ray spectroscopy and transmission electron microscopy (TEM). The $(Ru_xSn_{1-x})O_2$ was found to be a two-phase material consisting of probably a solid solution of RuO_2 in SnO_2 and pure RuO_2. The average Pt particle size determined by TEM was 5.3 nm. Cyclic voltammetry of Pt/$(Ru_xSn_{1-x})O_2$ indicated good conductivity of the support and displayed the usual features of Pt. The results of the electrochemical oxidation of CO_{ads} and methanol on Pt/$(Ru_xSn_{1-x})O_2$ were compared with those on commercial Pt/C and PtRu/C catalysts. Oxidation of CO_{ads} on Pt/$(Ru_xSn_{1-x})O_2$ starts at lower positive potentials than on PtRu/C and Pt/C. Potentiodynamic polarization curves and chronoamperometric curves of methanol oxidation indicated higher initial activity of the Pt/$(Ru_xSn_{1-x})O_2$ catalyst compared to PtRu/C, but also a greater loss in current density over time. A potentiodynamic stability test of the catalysts revealed that deactivation of Pt/$(Ru_xSn_{1-x})O_2$ and Pt/C was primarily caused by poisoning of the Pt surface by residues of methanol oxidation, which mostly occurred during the first potential cycle. In the case of PtRu/C, the poisoning of the surface was minor and deactivation was caused by surface area loss of the PtRu.

Keywords: methanol oxidation, CO oxidation, platinum, Ru-doped SnO_2, electrocatalysis, fuel cell.

* Corresponding author. E-mail: sgojkovic@tmf.bg.ac.rs
# Serbian Chemical Society member.
doi: 10.2298/JSC130718091K

INTRODUCTION

Anode and cathode catalysts currently used for polymer electrolyte membrane fuel cells (PEMFCs) are Pt or Pt-alloy nanoparticles supported on carbon blacks.[1] The role of the support for the catalysts is to provide a physical surface for a fine dispersion of catalyst particles, necessary to achieve a high surface area. To be efficient, the support also needs to have high surface area, preferably mesoporous structure, high electrical conductivity and high stability under fuel cell operating conditions.[2] The main drawback of carbon blacks, as well as other carbon materials (carbon fibers, carbon nanotubes, graphene), is their insufficient corrosion resistance.[2,3] Although the problem of instability of the supporting material is more prominent for a cathode catalyst because of its higher potential and the presence of H_2O_2 as a by-product of oxygen reduction, an anode catalyst could also be exposed to much more oxidative conditions in the case of cell reversal caused by fuel starvation.[4] Partial oxidation of the carbon induces the formation of oxygen-containing functional groups on the surface that weaken bonding with Pt nanoparticles, thus promoting surface diffusion of Pt nanoparticles and their agglomeration. If the carbon support is oxidized to CO or CO_2, Pt nanoparticles are detached from the surface.[3] In both cases, the final result is a decrease in the electrochemically active surface area of Pt. This problem has initiated a lot of research in the last few years aimed at finding an appropriate replacement for carbon supports. Ceramic materials, such as metal oxides and carbides, distinguish themselves as promising candidates not only due to their high stability in a fuel cell environment, but also because of their possible interaction with the deposited metal particles, which could result in a promotion of the activity of the catalyst.[2,5]

Metal oxides are electric insulators at the operating temperatures of PEMFCs. However, sub-stoichiometric oxides, oxides doped with a foreign metal and nanostructured oxides, especially those of titanium, tin and tungsten, are found to have acceptable conductivity for application as a support for electrocatalysts.[2] When using as an anode catalyst in a direct methanol or ethanol fuel cell (DMFC, DEFC), the metal-oxide support can also serve as a co-catalyst to Pt nanoparticles, providing them with oxygen-containing species at lower electrode potentials.

The state-of-the-art anode catalyst in DMFC is a Pt–Ru nanoalloy. It is accepted that the methanol oxidation reaction (MOR) commences earlier on Pt–Ru than on Pt due to the bi-functional mechanism,[6] according to which oxophilic Ru sites readily adsorb oxygen-containing species, which react with carbonaceous species formed by methanol adsorption on the Pt sites. Pt–Sn alloys were also investigated for the MOR, but found to be inactive.[7] Interestingly, good activity was observed for electrosorbed Sn on Pt.[7] It was also reported that tin oxide promotes the MOR on Pt, as shown for Pt microparticles dispersed on SnO_2 thin

films[8] and polycrystalline Pt partially covered by SnO_2 nanoparticles.[9] SnO_2 doped by Sb was investigated as a support for Pt nanoparticles.[10] It was concluded that Sb-doped SnO_2 promotes methanol and ethanol oxidation and stabilizes the Pt nanoparticles in the fuel cell.

In the present study, Pt nanoparticles supported on SnO_2 doped with RuO_2 were prepared. RuO_2 as a dopant should increase the electrical conductivity of SnO_2 and, together with SnO_2, provide oxygen-containing species necessary for efficient methanol oxidation on Pt. The supporting material, labeled as (Ru_xSn_{1-x})O_2, and the catalyst Pt/(Ru_xSn_{1-x})O_2 were characterized by the X-ray diffraction technique (XRD), transmission electron microscopy (TEM) and energy dispersive X-ray spectroscopy (EDS). The catalyst was tested for electrochemical oxidation of CO and methanol and its performance was compared to those of commercial Pt/C and PtRu/C catalysts.

EXPERIMENTAL

Synthesis of the support and the catalyst

The $Ru_xSn_{1-x}O_2$ supporting particles were prepared as follows.[11] A solution 5.3 g of $SnCl_4 \cdot 5H_2O$, 0.98 g of $RuCl_3 \cdot xH_2O$ (35–45 mass % Ru), 2.5 mL of HCl and 40 mL of high purity water (Millipore, 18 MΩ cm resistivity) was prepared and mixed to homogeneity. The mixture is added dropwise in 50 mL of a 34 % aqueous solution of hydrazine at room temperature. Then, the solution was refluxed for 10 days. Subsequently, the formed precipitate was repeatedly rinsed with water and centrifuged until the supernatant was free of Cl^-. The resulting product was dried in air for 24 h at 120 °C and heated at 400 °C for 2 h.

The Pt nanoparticles were deposited on the $Ru_xSn_{1-x}O_2$ support by a modified borohydride reduction method.[12] $Ru_xSn_{1-x}O_2$ powder was dispersed in water in an ultrasonic bath. Then H_2PtCl_6 aqueous solution was added into dispersion under continuous stirring. The metal salt was reduced with excess of sodium borohydride. The precipitate was rinsed with water and dried at 80 °C.

Physicochemical characterization

Adsorption and desorption isotherms of N_2 were measured on $Ru_xSn_{1-x}O_2$ support at –196°C, using the gravimetric McBain method. The BET specific surface area, S_{BET}, and pore size distribution were calculated from the isotherms. Pore size distribution was estimated by applying the BJH method[13] to the desorption branch of the isotherms.

Phase composition of the (Ru_xSn_{1-x})O_2 support was investigated by XRD technique. Siemens D-500 diffractometer was employed with CuK_α radiation of wavelength 0.154056 nm in conjunction with a CuK_β nickel filter.

Elemental analysis of the (Ru_xSn_{1-x})O_2 support and the Pt/$Ru_xSn_{1-x}O_2$ catalyst was performed by EDS analysis using a scanning electron microscope Tescan VEGA TS 5130MM coupled with an EDS system INCAPentaFET-x3, Oxford Instruments.

The Pt/(Ru_xSn_{1-x})O_2 catalyst was characterized for morphology, particle size distribution and chemical composition by TEM. The sample was sonicated in ethanol and a drop of the suspension was placed on copper grid (300 mesh) covered with a lacey carbon film and dried in air. A combination of high angle annular dark field scanning transmission electron microscopy (HAADF, STEM) and electron energy loss spectroscopy (EELS) was applied. HAADF was chosen because of its strong correlation between atomic number and image intensity,

making it very easy to distinguish between heavy elements, such as Pt, and light supports, such as $(Ru_xSn_{1-x})O_2$ particles. The measurements were performed on TEAM0.5 transmission electron microscope with corrected aberration operated at 80 kV. EDS analysis was performed on TEM microscope CM200-FEG operating at 400 kV using an Oxford Instruments EDS system with INCA software. Crystallographic information from individual Pt particles was obtained by numerical Fourier filtering (FFT, fast Fourier transformation) of the digital image intensity spectra. All TEM characterization was realized at the National Center for Electron Microscopy, Lawrence Berkeley National Laboratory, Berkeley, CA.

Electrochemical characterization

For the electrochemical characterization, the $Pt/(Ru_xSn_{1-x})O_2$ catalyst was applied on a glassy carbon (GC) substrate in the form of a thin-film.[14] The GC electrode (Tacussel rotating disk electrode, 5 mm in diameter) was polished with Al_2O_3 slurry and washed ultrasonically with water before use. The ink was made by mixing of 4 mg of $Pt/(Ru_xSn_{1-x})O_2$ powder with 1 cm^3 of high purity water and 50 μL of Nafion® solution (5 wt. %, 1100 E.W., Aldrich). After 1 h of agitation in an ultrasonic bath, 10 μL of the suspension was placed onto the GC electrode and left to dry overnight. This procedure of film preparation gave 60 μg of Pt per cm^2 of the GC surface.

Electrochemical characteristics of the $Pt/(Ru_xSn_{1-x})O_2$ thin film were investigated by cyclic voltammetry in 0.10 M H_2SO_4 saturated with N_2. After immersion into the electrolyte, the electrode was subjected to 15 potential cycles between 0.04 and 1.2 V at a scan rate of 100 mV s^{-1}. The oxidation of CO_{ads} was examined in the same electrolyte after adsorbing CO at 0.1 V for 30 min and replacing CO by a N_2 atmosphere.

The MOR was investigated in an electrolyte containing 0.5 M CH_3OH. Upon oxidation of CO_{ads}, the electrode potential was held at 0.1 V, methanol was added into the electrolyte and after 2 min a linear sweep at 50 mV s^{-1} (potentiodynamic polarization curve) or potential step at 0.5 V *vs*. RHE (chronoamperometric experiment) was applied.

As reference electrocatalysts, a sample of Pt nanoparticles supported on XC-72R carbon with a loading of 20 mass % of Pt (Pt/C) and a sample of PtRu nanoparticles supported on the same carbon with a loading of 20 mass % of PtRu (PtRu/C), both of them manufactured by E-Tek, were used. The average diameters of Pt and PtRu particles were 2.5[15] and 2.7 nm,[16] respectively. The metal loading on the electrode was 20 μg cm^{-2} for both Pt/C and PtRu/C.

The electrochemically active surface area of Pt and PtRu were determined from the charge of the CO_{ads} oxidation as well as from the charge of the oxidation of underpotentially deposited Cu.[17] Cu was deposited from a supporting electrolyte containing 2 mM $CuSO_4$ at a potential of 0.33 V.

A three-compartment electrochemical glass cell was used with a Pt wire as the counter electrode and a saturated calomel electrode as the reference electrode. All the potentials reported in the paper are expressed on the scale of the reversible hydrogen electrode (RHE). A Pine RDE4 potentiostat and Philips PM 8143 X–Y recorder were used. All the measurements were performed at 25 °C.

RESULTS AND DISCUSSION

Physicochemical characterization

Analysis of N_2 adsorption and desorption isotherms revealed that the $(Ru_xSn_{1-x})O_2$ powder had a BET surface area of 141 m^2 g^{-1} and mesoporous structure with pores radii mostly between 2 and 3 nm.

Both SnO_2 and RuO_2 crystallized in the tetragonal rutile structure with similar lattice constants (SnO_2: a = 0.47382 nm, c = 0.31871 nm; RuO_2: a = = 0.44994 nm, c = 0.31071 nm). The ionic radii of Sn(IV) and Ru(IV) of 0.083 and 0.076 nm are similar enough to enable the formation of a substitutional solid solution, designated as (Ru_xSn_{1-x})O_2.[18] The experimental XRD pattern for the (Ru_xSn_{1-x})O_2 support and the reference spectra of RuO_2 and SnO_2, taken from the corresponding JCPD cards, are shown in Fig. 1. The pattern for (Ru_xSn_{1-x})O_2 features overlapping peaks for SnO_2 and RuO_2. The 2θ peak positions and corresponding reflections for SnO_2 could be identified as 26.6° (110); 33.8° (101); 37.9° (200) 51.7° (211) and 64.7° (112) and for RuO_2 as 28.0° (110), 35.0° (101) and 54.2° (211). Such an XRD microstructure analysis suggests that (Ru_xSn_{1-x})O_2 consisted of two separate phases. Taking into account the possibility of the formation of a solid solution and greater amount of SnO_2, it could be suggested that the two phases detected by XRD were a solid solution of RuO_2 in SnO_2 and pure RuO_2.

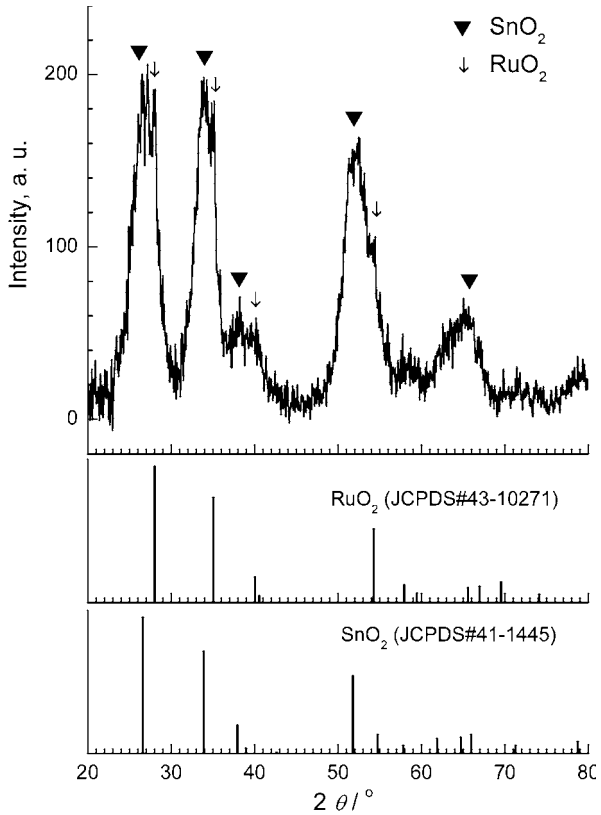

Fig. 1. XRD Pattern for the Pt/(Ru_xSn_{1-x})O_2 catalyst. The 2θ positions for bulk SnO_2 and RuO_2 are shown in the plot for reference.

EDS analysis revealed that the atomic ratio of Sn:Ru in the $(Ru_xSn_{1-x})O_2$ powder as well as in Pt/$(Ru_xSn_{1-x})O_2$ was 9:1. This shows that during the deposition of Pt nanoparticles on the $(Ru_xSn_{1-x})O_2$ support, its composition remained unchanged. The Pt loading of Pt/$(Ru_xSn_{1-x})O_2$ was found to be 30 mass %.

HAADF images of the Pt particles and the $(Ru_xSn_{1-x})O_2$ particle clusters are presented in Fig. 2a. It can be sees that Pt was unevenly distributed in the form of separate particles and particle clusters. The histogram given in Fig. 2b indicates the log–normal distribution of Pt particle size with an average size of 5.3 nm. Pt particles were mostly located near $(Ru_xSn_{1-x})O_2$ particle clusters, as presented in Fig. 2c and d, owing to the ability of SnO_2 to act as a nucleation agent. EELS analysis of the $(Ru_xSn_{1-x})O_2$ clusters revealed the presence of elemental Sn besides SnO_2. It could be assumed that Sn(IV) ions were partially reduced during Pt deposition by the borohydride reduction method.

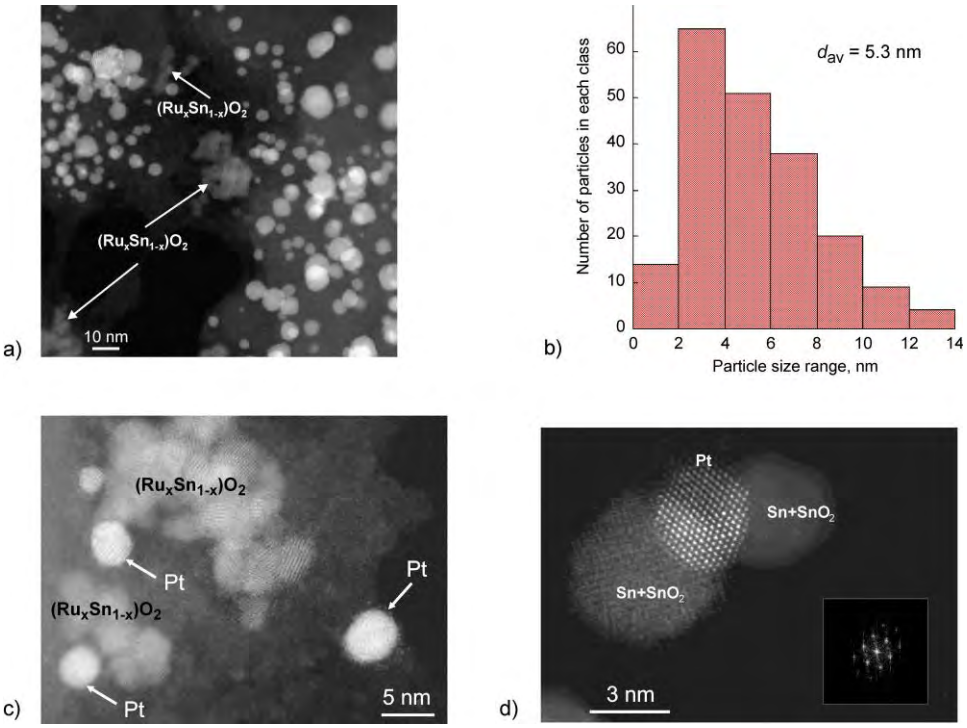

Fig. 2. TEM Images of the Pt/$(Ru_xSn_{1-x})O_2$ catalyst: a) HAADF image of the Pt particles and $(Ru_xSn_{1-x})O_2$ particle clusters, b) histogram of Pt particle size distribution, c) and d) close-up HAADF images of Pt particles close to $(Ru_xSn_{1-x})O_2$ particle clusters.

Cyclic voltammetry and CO_{ads} oxidation

The voltammograms of CO_{ads} stripping recorded on Pt/$(Ru_xSn_{1-x})O_2$, PtRu/C and Pt/C, as well as the first cyclic voltammograms after CO_{ads} stripping, are

shown in Fig. 3. The voltammograms after stripping of the CO_{ads} showed complete oxidation of the CO_{ads} and displayed the surface characteristics of the electrodes. The CO_{ads} stripping charge was used for the determination of the electrochemically active surface area (EASA) of Pt (in the case of Pt/(Ru_xSn_{1-x})O_2 and Pt/C) and PtRu (in the case of PtRu/C); hence, the current densities in Fig. 3 were normalized with respect to the EASA. It should be noted that the EASA values determined by the oxidation of underpotentially deposited monolayer of Cu (not shown) were the same, within experimental error, as those determined by oxidation of CO_{ads}.

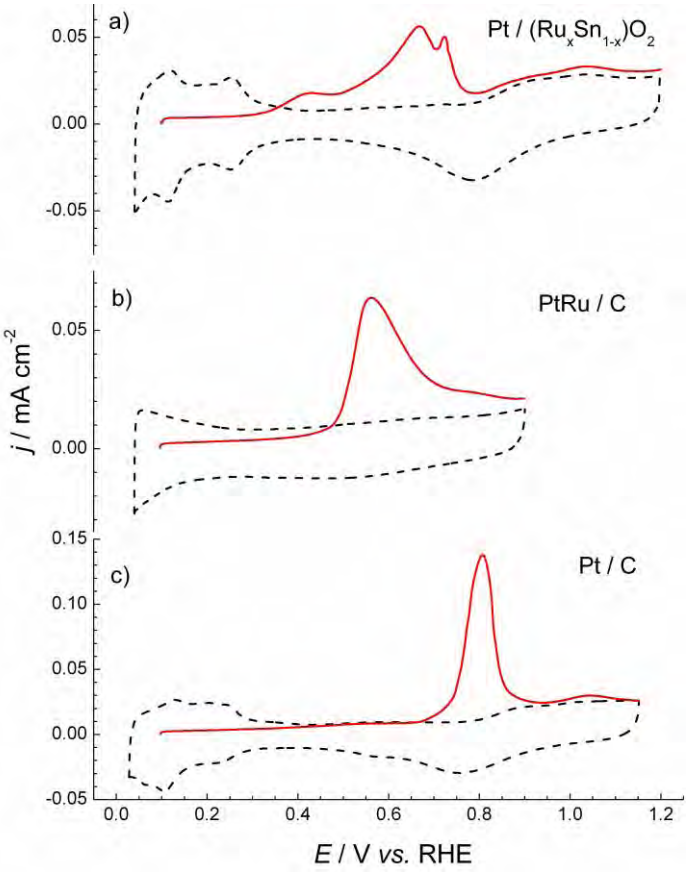

Fig. 3. Cyclic voltammograms of a) Pt/(Ru_xSn_{1-x})O_2, b) PtRu/C and c) Pt/C catalysts (dashed lines) and the corresponding stripping voltammograms of CO_{ads} (solid lines) recorded in 0.10 M H_2SO_4 at a scan rate of 20 mV s^{-1}.

The cyclic voltammogram of Pt/(Ru_xSn_{1-x})O_2 given in Fig. 3a shows well defined peaks for hydrogen adsorption/desorption and Pt-oxide formation/reduction that are characteristics of clean polycrystalline Pt. The high currents in the

so-called double-layer region of Pt can be mainly ascribed to the pseudo-capacitive behavior of the $(Ru_xSn_{1-x})O_2$ support. The voltammogram is well centered and without inclination, demonstrating good conductivity of the $(Ru_xSn_{1-x})O_2$ support.

Fig. 3a shows that CO_{ads} oxidation on Pt/$(Ru_xSn_{1-x})O_2$ occurred from 0.35 to 0.8 V. At low potentials, an anodic wave with a maximum at 0.43 V was observed. The main peak is a superposition of two peaks with maxima positioned at 0.70 and 0.72 V. Contrary to Pt/$(Ru_xSn_{1-x})O_2$, the voltammograms of the oxidation of CO_{ads} on PtRu/C (Fig. 3b) and Pt/C (Fig. 3c) showed single peaks. This suggested that the complex structure of the CO_{ads} oxidation voltammogram on Pt/$(Ru_xSn_{1-x})O_2$ was related to the presence of SnO_2. Indeed, a profile of CO_{ads} stripping with three peaks at almost the same potentials as those for Pt/$(Ru_xSn_{1-x})O_2$ was reported recently for Pt_3Sn/C catalyst containing Sn in the form of SnO_2.[19] On Pt_3Sn bulk alloy, it was also found that the CO_{ads} stripping begins at 0.25 V, but most of the CO_{ads} is oxidized in the second anodic wave starting at 0.68 V with the peak at about 0.75 V.[20] The authors assumed that a unique state of CO_{ads} existed on the Pt_3Sn surface, which is only formed at high coverage with an adsorption energy lower than that for pure Pt. Therefore, the first anodic wave in Fig. 3a could be ascribed to the oxidation of weakly bound CO_{ads} on the Pt sites directly contacting SnO_x, while the main peak corresponds to the oxidation of strongly bound CO_{ads}. The splitting of this peak might reflect CO_{ads} oxidation on Pt sites directly contacting SnO_x and the reaction on Pt sites completely surrounded by other Pt atoms. Comparing the CO_{ads} oxidation on Pt/$(Ru_xSn_{1-x})O_2$ to that on PtRu/C and Pt/C, the lowest onset potential on Pt/$(Ru_xSn_{1-x})O_2$ suggests that this catalyst should exhibit high CO tolerance.

Methanol oxidation

The activity of the catalysts for the MOR was first tested under potentiodynamic conditions. The polarization curves recorded in the positive going sweeps over 250 potential cycles are displayed in Fig. 4. The voltammograms recorded in the supporting electrolyte are also displayed. The Pt/$(Ru_xSn_{1-x})O_2$ catalyst features remarkably high current densities in the first potential cycle compared to Pt/C and especially to PtRu/C. Hydrogen desorption peaks were not attenuated, indicating that the electrocatalysts were not poisoned by the product of the dissociative adsorption of methanol during a 2-min potential hold at 0.1 V. However, already in the second cycle, the onset potential of the MOR on Pt/$(Ru_xSn_{1-x})O_2$ and Pt/C had shifted positively, probably as a consequence of poisoning of the Pt surface, which was evidenced by suppression of the hydrogen desorption peaks. Although the maximum current density on Pt/$(Ru_xSn_{1-x})O_2$ did not change with potential cycling, the activity at low potentials relevant for the operation of the anode in PEMFC was reduced. On the other hand, the activity of PtRu/C in the

first cycle was much lower than the activity of Pt/(Ru_xSn_{1-x})O_2 and Pt/C, but without significant loss of activity over the applied 250 potential cycles.

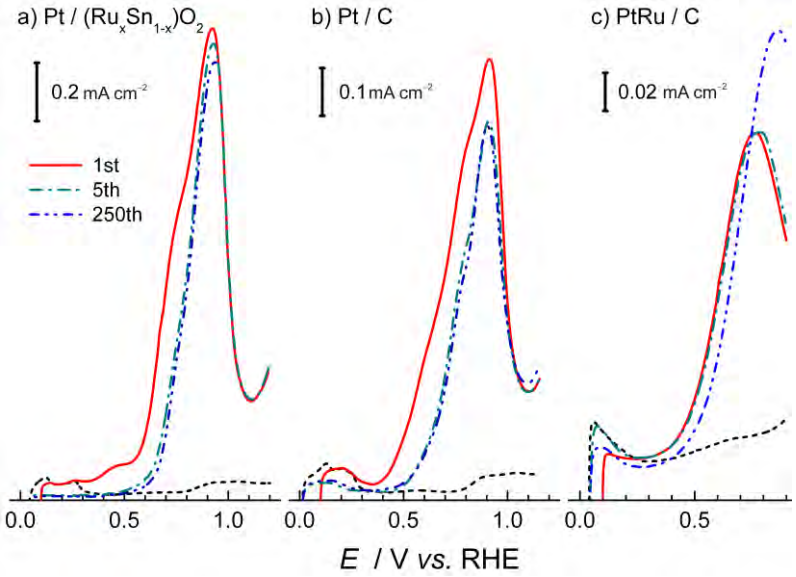

Fig. 4. Potentiodynamic polarization curves for the MOR recorded on a) Pt/(Ru_xSn_{1-x})O_2, b) Pt/C and c) PtRu/C in 0.1 M H_2SO_4 containing 0.5 M CH_3OH at a rate of 50 mV s^{-1} over 250 potential cycles. Anodic parts of the cyclic voltammograms recorded in 0.1 M H_2SO_4 before the addition of CH_3OH are also presented (dash line).

High activity of Pt/(Ru_xSn_{1-x})O_2 in the first cycle as well as the lower onset potential of CO_{ads} oxidation on this catalyst (Fig. 3a) compared to Pt/C and PtRu/C could be ascribed to SnO_x and its donation of oxygen-containing species. A recent investigation of CO and methanol oxidation on Pt partially covered by SnO_2 nanoparticles[9,21] showed that the lattice oxygen from Sn(II)O rather than Sn(IV)O is active in the oxidation of CO and methanol. This could suggest an explanation for the sharp drop in the activity for the MOR after the first cycle. Namely, during the 2 min potential hold at 0.1 V prior to the potential cycling experiment, the Sn(IV) ions in (Ru_xSn_{1-x})O_2 could be partially reduced to Sn(II) ions. If the partial reduction of Sn(IV) ions is a slow process, there is not enough time to form Sn(II) ions in the following continuous cycles.

The chronoamperometric test of Pt/(Ru_xSn_{1-x})O_2 and PtRu/C was performed at 0.50 V for 25 min. Similar to the findings of the potentiodynamic experiments, the chronoamperometric results (Fig. 5) confirmed the higher activity of the PtRu catalyst, but the difference in the activity between Pt/(Ru_xSn_{1-x})O_2 and PtRu/C slightly decreased during the experiment.

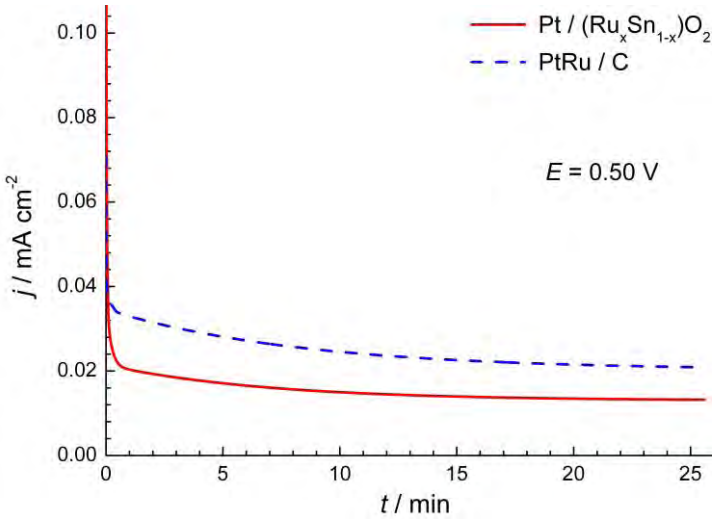

Fig. 5. Chronoamperometric curves of the MOR recorded on Pt/(Ru_xSn_{1-x})O_2 and PtRu/C catalysts in 0.1 M H_2SO_4 containing 0.5 M CH_3OH at a constant potential 0.50 V.

Stability of the catalysts

The activity of the catalysts for the MOR could deteriorate over time because of a gradual poisoning of the Pt surface by the methanol oxidation residues and/or because of a loss of the electrochemically active surface area. In order to resolve which effect was predominant, all three catalysts were subjected to potential cycling in the supporting electrolyte containing no methanol. At the beginning and at the end of the experiment, the procedure for CO adsorption was employed in order to determine the EASA. Additionally, for the Pt/(Ru_xSn_{1-x})O_2 catalyst, the EASA was continuously monitored by the changes in the hydrogen adsorption/desorption peaks. The changes in the Pt/(Ru_xSn_{1-x})O_2 cyclic voltammograms over 250 cycles are presented in Fig. 6. The currents in the hydrogen adsorption/desorption region as well as in the Pt-oxide formation/reduction region gradually decreased, revealing a loss of EASA. Degradation of Pt under the potentiodynamic conditions could be explained by two mechanisms; surface diffusion of low-coordinated Pt atoms[22] and electrochemical dissolution of Pt,[23–25] either as the direct electro-oxidation of Pt to soluble Pt^{2+} (mostly for particles smaller than 4 nm) or as dissolution from the oxide (larger particles).

It should be stressed that the voltammetric currents in the double-layer region, ascribed to pseudo-capacitive currents of the (Ru_xSn_{1-x})O_2 support (Fig. 6), do not change during potential cycling. Moreover, the characteristic shape of the voltammogram of CO_{ads} oxidation (Fig. 3a), which was related to the presence of SnO_x in the catalyst, was maintained over the potential cycling. The same shape of the CO_{ads} stripping curve before and after the stability test under the poten-

tiodynamic conditions was also reported for Pt_3Sn/C catalyst with Sn in a form SnO_2.[19] These results indicate that (Ru_xSn_{1-x})O_2 is a stable material and suitable for use as a catalyst support.

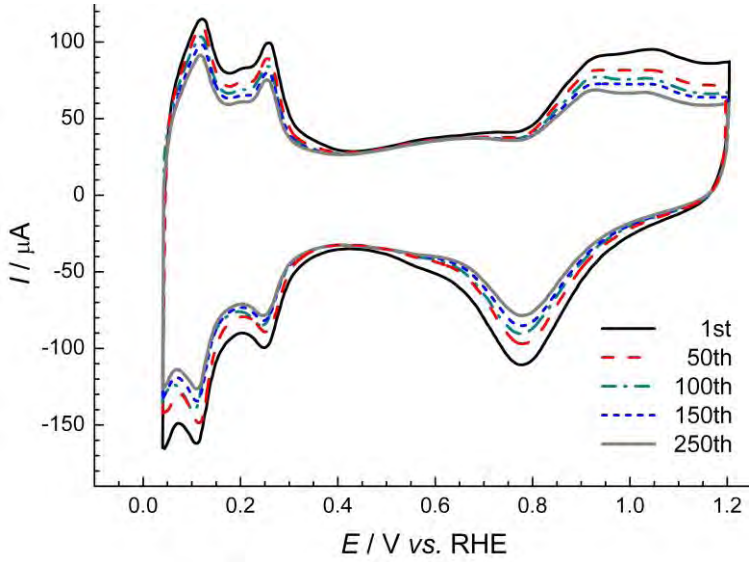

Fig. 6. Cyclic voltammograms of the Pt/(Ru_xSn_{1-x})O_2 catalyst recorded in 0.1 M H_2SO_4 at a scan rate of 50 mV s^{-1} over 250 cycles.

The EASA and the methanol oxidation current density for the Pt/(Ru_xSn_{1-x})O_2 catalyst collected over 250 potential cycles are shown in Fig. 7. The EASA data were determined from the hydrogen adsorption/desorption charge in all the cycles and from the CO_{ads} oxidation at the beginning and the end of the experiment. The values obtained by these two methods correspond to each other within experimental error. The current densities for the MOR were taken from the potentiodynamic curves in Fig. 4 at a constant potential of 0.50 V. They were calculated using the EASA at the beginning of the experiment. Both the EASA and the methanol oxidation current densities given in Fig. 7 were normalized with respect to their initial values. The results showed that 80 % of the initial activity for the MOR was lost while the EASA decreased by 32 %.

The results of the EASA and the MOR activity loss determined on all three catalysts are summarized in Table I. It is clear that the deactivation of the Pt/(Ru_xSn_{1-x})O_2 and Pt/C catalysts was primarily caused by the poisoning of the Pt surface by the methanol oxidation residues, mostly occurring during the first potential cycle (Fig. 4). Contrary to these two catalysts, for PtRu/C the loss of EASA and MOR activity were quite similar, indicating that poisoning of the PtRu nanoparticles was minor. Therefore, it seems that mixing of Pt and Ru at

the atomic level in necessary to achieve high and long-term resistance to poisoning by CO_{ads}.

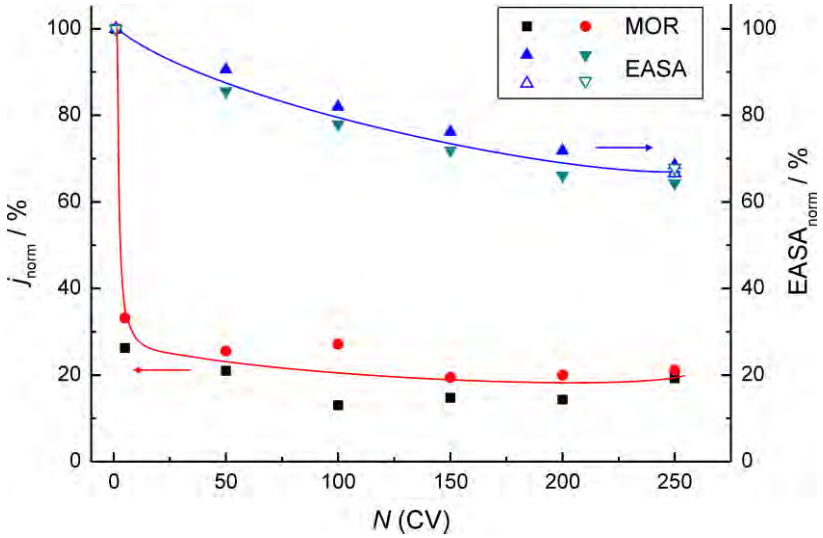

Fig. 7. The current densities for the MOR taken at 0.5 V and the EASA values during the potential cycling of $Pt/(Ru_xSn_{1-x})O_2$ in 0.1 M H_2SO_4 with and without 0.5 M CH_3OH. Both types of data are normalized to their initial values. EASA values were calculated from hydrogen desorption charge (bold symbols) and from CO_{ads} oxidation (open symbols). The results of two independent experiments are shown.

TABLE 1. Decrease in the activity for the MOR and the EASA values of the three investigated catalysts, determined during 250 potential cycles in 0.1 M H_2SO_4 solution with and without the addition of 0.5 M CH_3OH

Catalyst	MOR Activity loss, %	EASA Loss, %
$Pt/(Ru_xSn_{1-x})O_2$	80	32
Pt/C	70	18
PtRu/C	30	24

Prospects for the $Pt/(Ru_xSn_{1-x})O_2$ catalyst

The study of $Pt/(Ru_xSn_{1-x})O_2$ catalyst demonstrated that $(Ru_xSn_{1-x})O_2$ is stable within the potential range that might be encountered during the operation of a DMFC. This characteristic, as well as good conductivity, makes this oxide material suitable for application as a catalyst support.

The action of $(Ru_xSn_{1-x})O_2$ as co-catalyst is excellent in short time after running the MOR. However, very soon $Pt/(Ru_xSn_{1-x})O_2$ looses its high initial activity and the current densities for the MOR drop to 60 % of those attained on the commercial PtRu/C catalyst. Since the experiments show that $(Ru_xSn_{1-x})O_2$ cannot be an active co-catalyst to Pt over long-term operation, in further impro-

vement of the MOR catalyst without high area carbon as the support, PtRu nanoparticles could be deposited on a $(Ru_xSn_{1-x})O_2$ support.

Acknowledgement. This work was financially supported by the Ministry of Education, Science and Technological Development of the Republic of Serbia, Contract No. ON-172054.

ИЗВОД

ЕЛЕКТРОХЕМИЈСКА ОКСИДАЦИЈА МЕТАНОЛА НА КАТАЛИЗАТОРУ Pt/$(Ru_xSn_{1-x})O_2$

МИЛА Н. КРСТАЈИЋ[1], МАЈА Д. ОБРАДОВИЋ[2], БИЉАНА М. БАБИЋ[3], ВЕЛИМИР Р. РАДМИЛОВИЋ[1], УРОШ Ч. ЛАЧЊЕВАЦ[4], НЕДЕЉКО В. КРСТАЈИЋ[1] и СНЕЖАНА Љ. ГОЈКОВИЋ[1]

[1]*Технолошко–металуршки факултет, Универзитет у Београду, Карнегијева 4, 11000 Београд,* [2]*Институт за хемију, технологију и металургију, Универзитет у Београду, Његошева 12, Београд,* [3]*Институт за нуклеарне науке „Винча", Универзитет у Београду, п. пр. 522, Београд и* [4]*Институт за мултидисциплинарна истраживања, Универзитет у Београду, Кнеза Вишеслава 1, Београд*

Синтетизован је прах SnO_2 допован рутенијумом, $(Ru_xSn_{1-x})O_2$, са атомским односом Sn:Ru од 9:1, и коришћен као носач наночестица платине. Удео Pt у добијеном катализатору, Pt/$(Ru_xSn_{1-x})O_2$, био је 30 mas. %. Носач и катализатор су карактерисани дифракцијом X-зрака, енергетски дисперзивном спектроскопијом X-зрака и трансмисионом електронском микроскопијом (TEM). Показано је да је $(Ru_xSn_{1-x})O_2$ двофазни материјал који вероватно садржи чврст раствор RuO_2 у SnO_2 и чист RuO_2. Просечна величина зрна Pt, одређена TEM анализом, износи 5,3 nm. Циклична волтаметрија Pt/$(Ru_xSn_{1-x})O_2$ указала је на добру проводност носача катализатора и на уобичајене карактеристике Pt. Упоређени су резултати електрохемијске оксидације CO_{ads} на Pt/$(Ru_xSn_{1-x})O_2$, Pt/C и PtRu/C. Оксидација CO_{ads} на Pt/$(Ru_xSn_{1-x})O_2$ почиње на негативнијим потенцијалима у односу на PtRu/C и Pt/C. Потенциодинамичке поларизационе криве и хроноамперометријске криве за оксидацију метанола указују на већу почетну активност катализатора Pt/$(Ru_xSn_{1-x})O_2$ у односу на PtRu/C, али и на веће смањење густине струје током времена. Тест потенциодинамичке стабилности катализатора је указао да је смањење активности Pt/$(Ru_xSn_{1-x})O_2$ и Pt/C првенствено проузроковано тровањем површине Pt производима непотпуне оксидације метанола, које се углавном одиграва током првог циклуса. Код PtRu/C тровање површине је минимално, а смањење активности је проузроковано смањењем електрохемијски активне површине PtRu.

(Примљено 18. јула, ревидирано 4 септембра 2013)

REFERENCES

1. E. Antolini, *Appl. Catal., B* **88** (2009) 1
2. E. Antolini, E. R. Gonzales, *Solid State Ionics* **180** (2009) 746
3. J. Wang, G. Yin, Y. Shao, S. Zhang, Z. Wang, Y. Gao, *J. Power Sources* **171** (2007) 331
4. A. Taniguchi, T. Akita, K. Yasuda, Y. Miyazaki, *J. Power Sources* **130** (2004) 42
5. G. R. Dieckmann, S. H. Langer, *Electrochim. Acta* **44** (1998) 437
6. S. Wasmus, A. Küver, *J. Electroanal. Chem.* **461** (1999) 14
7. K. Wang, H. A. Gasteiger, N. M. Markovic, P. N. Ross Jr., *Electrochim. Acta* **41** (1996) 2587
8. A. L. Santos, D. Profeti, P. Olivi, *Electrochim. Acta* **50** (2005) 2615
9. W.-P. Zhou, W. An, D. Su, R. Palomino, P. Liu, M. G. White, R. R. Adzic, *J. Phys. Chem. Lett.* **3** (2012) 3286

10. K.-S. Lee, I.-S. Park, Y.-H. Cho, D.-S. Jung, H.-Y. Park, Y.-E. Sung, *J. Catal.* **258** (2008) 143
11. A. Hagemeyer, Z. Hogan, M. Schlichter, B. Smaka, G. Streukens, H. Turner, A. Volpe Jr., H. Weinberg, K. Yaccato, *Appl. Catal., A* **317** (2007) 139
12. K. W. Park, K. S. Seul, *Electrochem. Commun.* **9** (2007) 2256
13. E. P. Barret, L. G. Joyner, P. P. Halenda, *J. Am. Chem. Soc.* **73** (1951) 373
14. T. J. Schmidt, H. A. Gasteiger, R. J. Behm, *Electrochem. Commun.* **1** (1999) 1
15. I. Esparbé, E. Brillas, F. Centellas, J. A. Garrido, R. M. Rodríguez, C. Arias, P.-L. Cabot, *J. Power Sources* **190** (2009) 201
16. S. Lj. Gojković, T. R. Vidaković, D. R. Đurović, *Electrochim. Acta* **48** (2003) 3607
17. C. L. Green, A. Kucernak, *J. Phys. Chem., B* **106** (2002) 1036
18. X. Wang, F. Deng, Z. Tang, B. Wu, D. Tang, W. Linz, *Phys. Chem. Chem. Phys.* **15** (2013) 3977
19. E. Lee, A. Murthy, A. Manthiram, *J. Electroanal. Chem.* **659** (2011) 168
20. K. Wang, H. A. Gasteiger, N. M. Markovic, P. N. Ross, *Electrochim. Acta* **41** (1996) 2587
21. S. Axnanda, W.-P. Zhou, M. G. White, *Phys. Chem. Chem. Phys.* **14** (2012) 10207
22. Q. Xu, E. Kreidler, D. O. Wipf, T. He, *J. Electrochem. Soc.* **155** (2008) B228
23. L. Tang, B. Han, K. Persson, C. Friesen, T. He, K. Sieradzki, G. Ceder, *J. Am. Chem. Soc.* **132** (2010) 596
24. L. Tang, X. Li, R. C. Cammarata, C. Friesen, K. Sieradzki, *J. Am. Chem. Soc.* **132** (2010) 11722
25. A. A. Topalov, I. Katsounaros, M. Auinger, S. Cherevko, J. C. Meier, S. O. Klemm, K. J. J. Mayerhofer, *Angew. Chem Int. Ed.* **51** (2012) 12613.